Development 129, 3009-3019 (2002)
Printed in Great Britain © The Company of Biologists Limited 2002
DEV14536

DEVELOPMENT AND DISEASE

Disruption of *acvrl1* increases endothelial cell number in zebrafish cranial vessels

Beth L. Roman[1], Van N. Pham[1], Nathan D. Lawson[1], Magdalena Kulik[2,*], Sarah Childs[3,†], Arne C. Lekven[4,‡], Deborah M. Garrity[3], Randall T. Moon[4], Mark C. Fishman[3], Robert J. Lechleider[2,*] and Brant M. Weinstein[1,§]

[1]Laboratory of Molecular Genetics, National Institute of Child Health and Human Development, National Institutes of Health, Bethesda, MD 20892, USA
[2]Department of Pharmacology, Uniformed Services University of the Health Sciences, Bethesda, MD 20814, USA
[3]Cardiovascular Research Center, Massachusetts General Hospital East, Charlestown, MA 02129, USA
[4]Howard Hughes Medical Institute and Department of Pharmacology, University of Washington School of Medicine, Seattle, WA 98185 USA

*Present address: Department of Cell Biology, Georgetown University Medical School, Washington, DC 20007, USA
†Present address: Department of Biochemistry and Molecular Biology, University of Calgary, Calgary, AB T2N 4N1, Canada
‡Present address: Biology Department, Texas A&M University, College Station, TX 77843, USA
§Author for correspondence (e-mail: flyingfish@nih.gov)

Accepted 1 April 2002

SUMMARY

The zebrafish mutant *violet beauregarde* (*vbg*) can be identified at two days post-fertilization by an abnormal circulation pattern in which most blood cells flow through a limited number of dilated cranial vessels and fail to perfuse the trunk and tail. This phenotype cannot be explained by caudal vessel abnormalities or by a defect in cranial vessel patterning, but instead stems from an increase in endothelial cell number in specific cranial vessels. We show that *vbg* encodes activin receptor-like kinase 1 (Acvrl1; also known as Alk1), a TGFβ type I receptor that is expressed predominantly in the endothelium of the vessels that become dilated in *vbg* mutants. Thus, *vbg* provides a model for the human autosomal dominant disorder, hereditary hemorrhagic telangiectasia type 2, in which disruption of *ACVRL1* causes vessel malformations that may result in hemorrhage or stroke.

Movies available on-line

Key words: Acvrl1, Hereditary hemorrhagic telangiectasia, Endothelium, Angiogenesis, Zebrafish, *violet beauregarde*

INTRODUCTION

The mechanism by which the embryonic vasculature forms can be divided into two major processes: vasculogenesis and angiogenesis. In vasculogenesis, mesodermally derived endothelial cell precursors or angioblasts migrate to future vessel sites and coalesce with neighbors to form endothelial cell cords, which lumenize and become ensheathed by supporting smooth muscle cells or pericytes. This primitive vascular network provides the substrate for angiogenic processes, which include remodeling of vasculogenic vessels, sprouting of new vessels, and intussusception, which facilitates vessel branching.

A number of ligand/receptor pairs have been identified that help to coordinate vasculogenesis and angiogenesis. These include vascular endothelial growth factor (VEGF) and VEGF receptor 2 (VEGFR2); angiopoietins 1 and 2 and the Tie2 receptor; ephrin-B2 and EphB4; and platelet-derived growth factor B (PDGFB) and PDGF receptor β. Of these, only VEGF and VEGFR2 are required for both vasculogenesis and angiogenesis, whereas the rest play roles in angiogenic processes and/or perivascular sheath formation (for review, see Roman and Weinstein, 2000). TGFβ family signaling is also important in blood vessel development, although the precise ligand/receptor pairs and their specific roles are not well established. TGFβ family ligands bind to a heterodimeric complex consisting of a type II and a type I receptor, both of which are transmembrane serine/threonine kinases (for review, see Massague et al., 2000). Ligand binding stimulates the type II receptor to phosphorylate the type I receptor, which in turn phosphorylates a receptor-specific Smad. This phosphorylated Smad dimerizes with a common partner Smad (Smad4), forming a complex that translocates to the nucleus and directly regulates gene transcription. TGFβ family ligands can be divided into two groups based on Smad specificity: TGFβs, activins, and nodals signal through Smad2 and Smad3, whereas bone morphogenetic proteins (BMPs) signal through Smad1, Smad5, and Smad8.

The importance of TGFβ family signaling in vessel

development is illustrated by the following observations. Targeted deletion of *Tgfb1* impairs yolk sac vasculogenesis but has no effect on vasculogenesis or angiogenesis within the embryo proper (Dickson et al., 1995). A similar extraembryonic vascular phenotype, characterized by dilated vessels that exhibit poor endothelial cell adhesion and impaired vascular smooth muscle development, results from targeted disruption of TGFβ receptor II (*Tgfbr2*) or TGFβ receptor I (*Tgfbr1*), which together constitute the canonical receptor pair for TGFβ1 (Larsson et al., 2001; Oshima et al., 1996). In addition to defects in yolk sac vasculogenesis, angiogenic defects are observed within the embryo proper in *Tgfbr2* null mice (R. J. L., unpublished observation) and within the embryonic portion of the placenta in *Tgfbr1* null mice (Larsson et al., 2001). Furthermore, disruption of *endoglin* (*Eng*), an accessory receptor that binds TGFβs, activins, and BMPs (Barbara et al., 1999), impairs primitive plexus remodeling and vascular smooth muscle differentiation both in the yolk sac and within the embryo proper (Li et al., 1999). Targeted disruption of *Acvrl1*, a TGFβ type I receptor that signals through Smad1/5/8 (Chen and Massague, 1999), or disruption of *Smad5* itself, results in extraembryonic and intraembryonic vessel dilation, defects in vascular plexus remodeling, and impaired vascular smooth muscle differentiation (Oh et al., 2000; Urness et al., 2000; Yang et al., 1999). The ligand involved in this Acvrl1-Smad1/5/8 pathway is not clear but may be TGFβ1, which has been shown to bind Acvrl1 and TGFβRII (Lux et al., 1999; Oh et al., 2000) and to stimulate Smad1 phosphorylation (Yue et al., 1999) in vitro. However, no downstream targets of TGFβ1-stimulated Acvrl1 signaling have been identified.

In humans, mutations in *ENG* and *ACVRL1* are responsible for the autosomal dominant vascular dysplasias, hereditary hemorrhagic telangiectasia (HHT) type 1 and type 2, respectively (Johnson et al., 1996; McAllister et al., 1994), which together occur with a frequency of 1 in 10,000 (McDonald et al., 2000). These diseases present clinically in a similar manner, with symptoms including epistaxis (recurrent nosebleeds), mucocutaneous telangiectases (superficial vascular dilations that present as small red spots), and arteriovenous malformations (AVMs) (Guttmacher et al., 1995). Large AVMs, particularly in brain and lung, can lead to stroke if severe shunting or rupture occurs. The basis for the localized nature of these defects is not known, although it has been suggested that the appearance of pathological lesions is precipitated by some independent, site-specific event (Guttmacher et al., 1995). The age of onset and expressivity of these diseases are highly variable and seem to depend on both genetic and epigenetic factors.

In the current study, we present a new vertebrate model for HHT2: the zebrafish mutant, *violet beauregarde* (*vbg*). In homozygous *vbg* mutants, the majority of blood flow is confined to a small number of dilated cranial vessels that contain more than twice as many endothelial cells as their wild-type counterparts. The *vbg* locus maps to linkage group (LG) 23 and encodes Acvrl1, which is expressed predominantly in the endothelium of those cranial vessels that are dilated in *vbg* mutants. As Acvrl1 ligand(s) and downstream targets of Acvrl1 signaling are presently ill-defined, the embryological, molecular and molecular genetic techniques afforded by the zebrafish system make the *vbg* mutant a valuable model for dissecting the molecular pathway by which Acvrl1 directs embryonic vessel formation, which in turn could lead to insight into the molecular mechanisms responsible for HHT2 pathogenesis.

MATERIALS AND METHODS

Zebrafish lines and maintenance

Adult zebrafish (*Danio rerio*) were maintained as described (Westerfield, 1995). vbg^{y6} and vbg^{ft09e} were isolated from independent ethylnitrosourea (ENU) mutagenesis screens on AB (Driever et al., 1996) and TL (Chen et al., 2001) backgrounds, respectively. $vbg^{df(LG23)w5}$ was isolated from a gamma ray mutagenesis screen on AB background (Lekven et al., 2000). Mapping lines were generated by outcrossing vbg^{y6} heterozygotes to a Hong Kong strain. The transgenic lines $TG(fli1{:}EGFP)^{y1}$ and $TG(fli1{:}nEGFP)^{y7}$, expressing cytoplasmic or nuclear-localized EGFP under the control of an 18 kb (N. D. L. and B. M. W., unpublished) or 7 kb (Lawson et al., 2001) fragment of the zebrafish *fli1* promoter, respectively, were generated as described (N. D. L. and B. M. W., unpublished). Both *fli1* promoter fragments direct transgene expression to migrating angioblasts, endothelial cells, early blood cells and pharyngeal arch mesenchyme. Mutant transgenic lines were generated by outcrossing transgenics to $vbg^{y6/+}$ or $vbg^{ft09e/+}$. Embryos were raised and staged as described previously (Kimmel et al., 1995; Westerfield, 1995). Embryo medium was supplemented with 0.003% phenylthiourea (Sigma) at 24 hours post-fertilization (hpf) to prevent melanin formation (Westerfield, 1995).

Microangiography and confocal imaging

Microangiography was performed as described (Weinstein et al., 1995). For confocal microscopy, embryos were anesthetized using 0.016% Tricaine (Sigma), mounted on depression slides using 5% methylcellulose (Sigma), and Z-series of frame-averaged optical sections were generated using a Radiance 2000 confocal microscope (Bio-Rad). Two-dimensional and three-dimensional projections were generated using MetaMorph (Universal Imaging) software.

Nuclei counting

The basal communicating artery and posterior connecting segments (Isogai et al., 2001) were imaged by confocal microscopy at 2 and 3 days post-fertilization (dpf) in embryos derived from $vbg^{ft09e/+}{;}TG(fli1{:}nEGFP)^{y7}$ incrosses. Cell number within these vessels was analyzed in 12 wild-type and 12 mutant embryos by counting nuclei on three-dimensional, rotating projections using the 'Manually Count Objects' function in MetaMorph. Data were analyzed by repeated measures ANOVA.

Meiotic and physical mapping

Embryos used for meiotic mapping were digested overnight at 50°C in 100 μl of buffer containing 10 mM Tris, pH 8.0; 50 mM EDTA; 200 mM NaCl; 0.5 mg/ml proteinase K; and 0.5% SDS. Digests were spun through Sephacryl-S400 (Amersham Pharmacia), and the resulting preparation of genomic DNA was used for PCR. SSLP mapping was performed as described previously (Knapik et al., 1998) except primers were not radiolabeled and PCR reactions were resolved on 3% MetaPhor agarose gels (FMC). YAC clones were identified from DNA pools by PCR as described by the supplier (Invitrogen) and isolated in agarose plugs and sized by standard techniques. For PCR and end rescue, agarose plugs were equilibrated in TE, pH 8.0, and YAC DNA was purified using the Qiaquick gel extraction kit (Qiagen). YAC ends were rescued by digesting this preparation with either *Bam*HI or *Spe*I and self-ligating to form transformable plasmids. BAC clones were identified from DNA pools by PCR as described by the supplier (Incyte Genomics), and prepared using Nucleobond columns (Clontech). Sequencing was performed

using BigDye reagents on an ABI310 capillary sequencer (Perkin-Elmer). PCR primers designed against non-repetitive regions of YAC and BAC DNA shown to be present on LG23 by radiation hybrid mapping (Hukriede et al., 1999) were used to establish physical contigs and to look for polymorphisms for use in meiotic mapping. To find polymorphisms, PCR products amplified from genomic DNA from individual wild-type, heterozygous and mutant embryos (genotype based on flanking markers) were sequenced. Single nucleotide polymorphisms were assayed as restriction fragment length polymorphisms (RFLPs), when possible, or were converted to RFLPs using derived cleaved amplified polymorphic sequence (dCAPS) analysis (Neff et al., 1998). One novel SSLP (bac156CA) was identified in BAC156f04 as described previously (Knapik et al., 1998).

Cloning of zebrafish *acvrl1* cDNA

A tblastn search uncovered a 3′ zebrafish EST, *zehn1109*, with homology to human ACVRL1. 5′ SMART RACE (Clontech) was performed using first strand cDNA synthesized from total RNA from 24 hpf embryos and a *zehn1109*-specific primer, 5′-CCTCT-GGTGCCATGTATCGCTTG-3′. Analysis revealed two RACE products that diverged five bases 5′ of the putative start codon (see Results). cDNA was synthesized from RNA obtained from wild-type, vbg^{y6}/vbg^{y6}, and vbg^{ft09e}/vbg^{ft09e} embryos using SuperscriptII (Life Technologies), and PCR was performed using PLATINUM *Pfx* DNA polymerase (Life Technologies) and primers specific to the 5′ UTR of the major RACE product (f9: 5′-TTGCCGCCCGTTATGAGAAT-3′) and the 3′ UTR of *zehn1109* (r9: 5′-TCGGTGGAGCCTAA-GGACAAGAAG-3′). A single product was obtained, cloned into pCRII-TOPO (Invitrogen), and sequenced. The G→T transversion found in vbg^{y6} was assayed by dCAPS analysis using the following primers: 5′-CACGGTCCAACTAAGGCATGAAAACACCTT-3′, 5′-GTGTGCTATGGCTGGTTTG-3′. The forward primer ends just 5′ to the mutation and contains a single mismatch (underlined) that creates a *Bsa*JI site in the wild-type sequence.

In situ hybridization and immunohistochemistry

Whole-mount in situ hybridization was performed as described previously (Hauptmann and Gerster, 1994). For *acvrl1* detection, a PCR fragment was amplified from 24 hour cDNA (5′-GGCCC-TGGGTCTCGTCTT-3′ and 5′-AACCCCATCTTACCCTCACTTT-AC-3′) and cloned into pCRII-TOPO (Invitrogen). Other probes used were *tie1* (Lyons et al., 1998), *gata2* (Detrich et al., 1995), and *ephrin-b2* (kindly provided by M. Tsang). Whole-mount immunohistochemistry was performed using the Vectastain Elite ABC kit (Vector Laboratories) as described by Westerfield (Westerfield, 1995). Rabbit polyclonal phospho-Smad1 antibody (Cell Signaling Technology) was used at 1:1500. Mouse monoclonal myc antibody (Babco) was used at 1:2000.

Expression constructs and morpholinos

The *acvrl1* pCRII-TOPO clones described above (wild-type and vbg^{y6} alleles) were used as templates in a PCR using primer f9 extended with a *Bam*HI site (5′-TATAGGATCCTTGCCGCCCGTTATGA-GAATAC-3′), and primer r9 extended with a *Cla*I site (5′-TATAATCGATCGAGGTCCAGTTTAAGCTTGTCTATG-3′). The resulting product was digested with *Bam*HI and *Cla*I and cloned into *Bam*HI/*Cla*I-digested pCS2+ upstream of a six-myc tag (pCS2+MT) (Rupp et al., 1994). Activated, myc-tagged constructs were generated by PCR using the QuikChange kit (Stratagene), *acvrl1*-pCS2+MT clones, and the following complementary primers: 5′-GCAGAG-GACCATGGCGCGAGATATCTCTCTGGTTGAGTG-3′, and 5′-CACTCAACCAGAGAGATATCTCGCGCCATGGTCCTCTGC-3′. These primers contain two mismatches (underlined), converting glutamine 193 (CAG) to aspartic acid (GAT). Dominant-negative, myc-tagged constructs were similarly generated using complementary primers 5′-GAAAGTGTGGCTGTCAGGATTTTCTCCTCTCGTG-ATG-3′, and 5′-CATCACGAGAGGAGAAAATCCTGACAGCCA-CACTTTC-3′. These primers contain a single mismatch (underlined), converting lysine 221 (AAG) to arginine (AGG). All constructs were verified by sequencing. Capped mRNA was synthesized from *Not*I-digested constructs using mMessage mMachine with SP6 RNA polymerase (Ambion). Morpholino-modified antisense oligonucleotides (Gene Tools) used were standard control (5′-CC-TCTTACCTCAGTTACAATTTATA-3′); MO1 (5′-CTGCGAGCAT-CACTGAAGCCTTC-3′), which targets +3 to +25 of the coding region of *acvrl1*; and MO2 (5′-CTCATTACTCAAACATAGAAGT-GTA-3′), which targets –95 to –71 of the major *acvrl1* splice variant containing noncoding exon1. Capped mRNAs and morpholinos were injected into 1- to 4-cell embryos either into a single blastomere or into the streaming yolk cytoplasm, just beneath the blastomeres, as described previously (Westerfield, 1995).

Luciferase reporter assays

P19 cells maintained in DMEM with 10% fetal bovine serum and antibiotics were transiently transfected with Smad2/3-responsive *pA3-lux* or Smad1/5/8-responsive *pTLX2-lux* (luciferase reporters) and the indicated activated TGFβ type I receptor constructs by calcium phosphate precipitation as described (Macias-Silva et al., 1998). One day following transfection, cells were placed in 0.2% serum in DMEM, and luciferase activity was determined using the Dual-Luciferase Reporter Assay System (Promega). For each experiment, transfections were performed in triplicate, and each well was assayed for luciferase activity in duplicate. Experiments were repeated at least three times with similar results. Data are expressed in relative luciferase units and were compared by Cochran's *t*-test.

RESULTS

vbg mutants exhibit abnormal circulation in the presence of normal vessel patterning

In zebrafish, trunk circulation begins between 24 and 26 hpf. A few hours later, perfusion of the head is initiated (Isogai et al., 2001). At these early stages, when heartbeat is weak and blood flow is slow, *vbg* mutants cannot be distinguished from their wild-type siblings. However, by 36-40 hpf, as the heartbeat quickens and strengthens and the number of circulating blood cells increases, most *vbg* mutants exhibit slightly weaker trunk circulation than wild-type siblings. By 2 dpf, although a few blood cells slowly traverse the trunk and tail in *vbg* mutants, most are restricted to a loop of dilated cranial vessels (Movies 1,2; http://dev.biologists.org/supplemental/). The anterior limit of this vessel loop lies medial to the center of the eye, the dorsal limit lies medial to the otic vesicle, and the posterior limit lies just posterior to the otic vesicle. Homozygous *vbg* mutants become progressively edematous in the head, pericardium and yolk sac (Fig. 1A,B) and die between 7 and 10 dpf. Thus far, three *vbg* alleles have been identified: vbg^{y6} (Driever et al., 1996) and vbg^{ft09e} (Chen et al., 2001) were isolated in independent ENU mutagenesis screens, and $vbg^{df(LG23)w5}$ was isolated in a gamma ray mutagenesis screen and represents a deletion (Lekven et al., 2000). With respect to vascular phenotype, the three *vbg* alleles are essentially indistinguishable (see below).

In order to directly compare the patent vasculature in wild-type and *vbg* mutant zebrafish, we employed confocal microangiography (Weinstein et al., 1995). In the 2.25 dpf wild-type zebrafish (Fig. 1C,D), blood flows caudally through the lateral dorsal aortae, as well as rostrally, through the

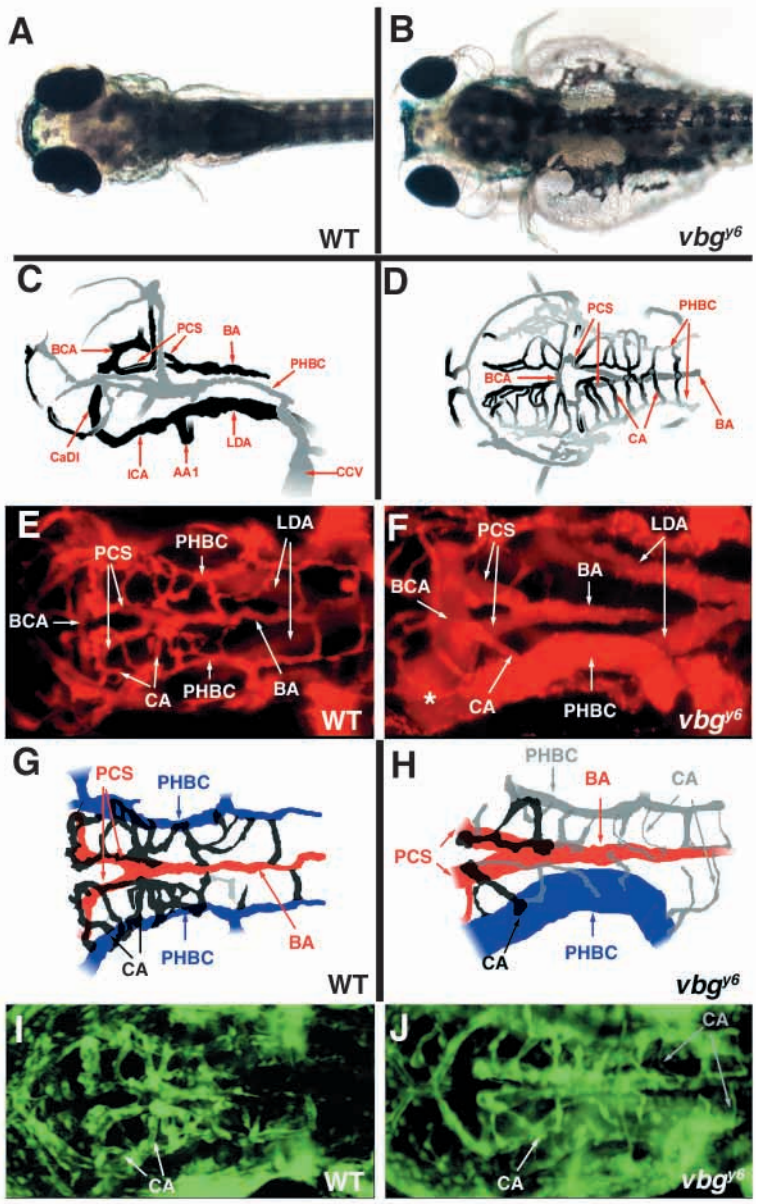

Fig. 1. *vbg* mutants exhibit abnormal circulation in the absence of vessel patterning abnormalities. (A) Wild-type zebrafish at 5 dpf. (B) *vbg*^{y6} mutant at 5 dpf. Note edema in the head, pericardium, and yolk sac. This edema is associated with an abnormal circulation pattern in which most blood flows through a limited number of dilated cranial vessels, with little to no circulation through the trunk and tail (Movies 1,2; http://dev.biologists.org/supplemental/). (C,D) Schematic diagrams of the vasculature in the 2.25 dpf wild-type zebrafish head. See text for detailed explanation. (E) Dorsal anterior angiogram of a *vbg*$^{+}$*;TG(fli1:EGFP)*^{y1} wild-type embryo at 2.25 dpf. Note the prominent central arteries (CA) and the relatively small caliber of the basal communicating artery (BCA), posterior connecting segments (PCS), basilar artery (BA), and primordial hindbrain channels (PHBC). (F) Dorsal anterior angiogram of a *vbg*^{y6}*;TG(fli1:EGFP)*^{y1} mutant at 2.25 dpf. Note the limited number of patent CAs, the enlarged vessels (BCA, PCS, BA, and PHBC), and the retention of a normally transient connection (*) between the BCA and the left PHBC. (I) *fli1* promoter-driven EGFP expression in the same wild-type embryo shown in E. (J) *fli1* promoter-driven EGFP expression in the same *vbg*^{y6} mutant shown in F. (G) Tracing of wild-type vasculature from images shown in E,I. (H) Tracing of *vbg*^{y6} mutant vasculature from images shown in (F,J). Patent vessels in G,H are black, blue, or red; solid cords are gray. While there is no difference in CA number or pattern, almost all CAs are patent in wild-type embryos, whereas most are not patent in *vbg* mutants (see also gray arrows, J). AA1, first arch artery; LDA, lateral dorsal aortae; ICA, internal carotid artery; CaDI, caudal division of ICA; (A,B,D-J) Dorsal view, anterior to the left. (C) Dorsolateral view, anterior to the left.

internal carotid arteries. Each internal carotid artery divides at the base of the eye into a cranial division, which continues rostrally, and a caudal division, which turns dorsally, behind the eye. The left and right caudal divisions of the internal carotid artery are connected beneath the midbrain via the basal communicating artery. From the basal communicating artery, blood flows through bilateral posterior connecting segments into the midline basilar artery, which runs beneath the hindbrain, and drains to the bilateral primordial hindbrain channels (primitive veins) through central arteries, which penetrate the hindbrain. Confocal microangiography clearly highlights this network of cranial vessels in wild-type zebrafish (Fig. 1E). In contrast, angiograms of all three *vbg* mutant alleles reveal a cranial vasculature containing dilated major vessels and very few patent central arteries (Fig. 1F and data not shown) compared to wild-type siblings, although trunk and tail vasculature appear normal (data not shown). The first arch artery and internal carotid artery/caudal division are greatly dilated in *vbg* mutants (Movie 1; http://dev.biologists.org/supplemental/), as are the basal communicating artery, posterior connecting segments, basilar artery, and left and/or right primordial hindbrain channels (Fig. 1F). The random retention of normally transient connections between the basal communicating artery and the left and/or right primordial hindbrain channel (Fig. 1F, Fig. 4B), or between the basilar artery and the primordial hindbrain channel (comparable to Fig. 4C), underlies the variability in patent cranial vessel architecture observed in *vbg* mutants.

To determine whether the defects noted in patent vessels in *vbg* mutants stem from defects in cranial vascular patterning, we used confocal microscopy to analyze the vasculature of transgenic fish [*TG(fli1:EGFP)*^{y1}] expressing EGFP under the control of the *fli1* promoter (N. D. L. and B. M. W., unpublished). Simultaneous analysis of endothelial structures (EGFP) and patent vasculature (microangiography) in wild-type and *vbg* embryos reveals no difference in vessel patterning (Fig. 1I,J) despite striking differences in vessel caliber and patency (Fig. 1E,F). These data might suggest that the *vbg* mutation-associated change in vascular hemodynamics stems from a defect in central artery lumenization (Fig. 1G,H). However, enlarged cranial vessels in *vbg* mutants can be seen by angiography as early as 40 hpf, a time at which central arteries are not patent in wild-type fish. Therefore, it is likely that cranial vessel enlargement and not impaired central artery lumenization is the proximal vascular defect in *vbg* mutants.

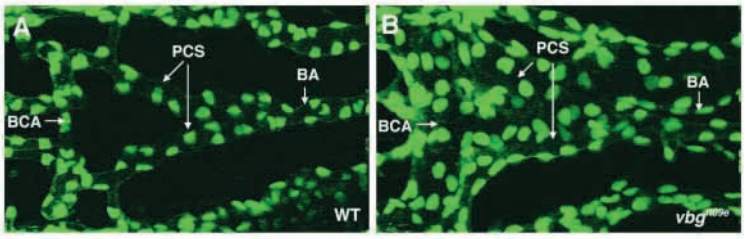

Fig. 2. Disruption of *acvrl1* increases the number of endothelial cells in the basal communicating artery (BCA) and posterior connecting segments (PCS) at 2-2.25 dpf. (A,B) Representative confocal micrograph of the central cranial vasculature of (A) a *vbg*$^{+}$*;TG(fli1;nEGFP)*^{y7} wild-type embryo, and (B) a *vbg*^{ft09e}*;TG(fli1;nEGFP)*^{y7} mutant embryo. The greater than two-fold increase in endothelial cell number in the BCA/PCS in *vbg*^{ft09e} embryos compared to wild-type embryos is significant at $P<0.00001$. BA, basilar artery. Dorsal views, anterior to the left.

Cranial vessel enlargement in *vbg* mutants stems from an increase in endothelial cell number

In order to determine whether cranial vessel dilation in *vbg* mutants involves endothelial cell hypertrophy or an increase in endothelial cell number, we counted nuclei in the vascular triangle comprising the basal communicating artery and posterior connecting segments. These vessels were chosen for analysis because they are consistently dilated in *vbg* mutants and are easily imaged in *TG(fli1:nEGFP)*^{y7} embryos. (Strong expression of the *fli1:nEGFP* transgene in pharyngeal arch mesenchyme precludes visualization of endothelial nuclei in the first arch artery and the internal carotid artery/caudal division.) Within this vessel triangle at 2-2.25 dpf, wild-type embryos have 32.9±1.0 (mean±s.e.m., n=12) endothelial nuclei (Fig. 2A), whereas *vbg* mutants have 69.8±2.6 (mean±s.e.m., n=12) endothelial nuclei (Fig. 2B). This greater than 2-fold increase in endothelial cell nuclei in *vbg* mutants persisted at 3 dpf, at which time endothelial cell number was statistically unchanged compared to 2 dpf (data not shown).

The *vbg* gene encodes Acvrl1

In order to determine the molecular basis for the increase in endothelial cell number in specific cranial vessels in *vbg* mutants, we positionally cloned the *vbg* locus. Analysis of simple sequence length polymorphisms (SSLPs) in pooled genomic DNA from phenotypically wild-type and mutant embryos from *vbg*$^{y6/+}$ incrosses placed *vbg* on LG23, and fine mapping defined an approximately 1 centimorgan (cM) meiotic interval between z14967 and z4421 (Fig. 3). A physical contig anchored at the z14967-end of the interval was generated, and meiotic mapping of single nucleotide polymorphisms narrowed the critical interval to 0.035 cM: the distance between markers b82sp6 and *taram-a*. Analysis of 4256 mutant embryos (8512 informative meioses) failed to further narrow the interval, which was spanned by BAC177k23 and BAC157p19.

Because *Acvrl1* disruption causes vascular defects in mice and humans (Johnson et al., 1996; Oh et al., 2000; Urness et al., 2000), and because human *ACVRL1* maps to chromosome 12q13, a region that shows conserved synteny with zebrafish LG23 (Postlethwait et al., 1998), *acvrl1* was tested as a candidate for *vbg*. A database search uncovered a 3′ zebrafish EST, *zehn1109*, with significant homology to the kinase domain of mammalian *Acvrl1*. Two independent PCR primer sets designed within the 3′UTR of this gene amplified fragments of the expected size from YAC35b1, BAC177k23, BAC157p19, and BAC143a24. The 5′ end of *zehn1109* was obtained by RACE and a primer made against the 5′UTR was successfully used in sequencing BAC177k23 but not BAC157p19 or BAC143a24. Therefore, the entire *zehn1109* gene is present within the critical interval, on BAC 177k23, and is absent from genomic DNA from *vbg*$^{df(LG23)w5}$ mutants (Fig. 3). It should be noted that, using RACE, two populations of 5′ clones were obtained that diverged at –5 with respect to the putative translational start codon. The most abundant fragment (5 out of 6 clones) contained a non-coding first exon, whereas the rare fragment (1 out of 6 clones) did not contain this exon. This phenomenon has also been reported for human *ACVRL1* (Berg et al., 1997).

Conceptual translation of the largest open reading frame of

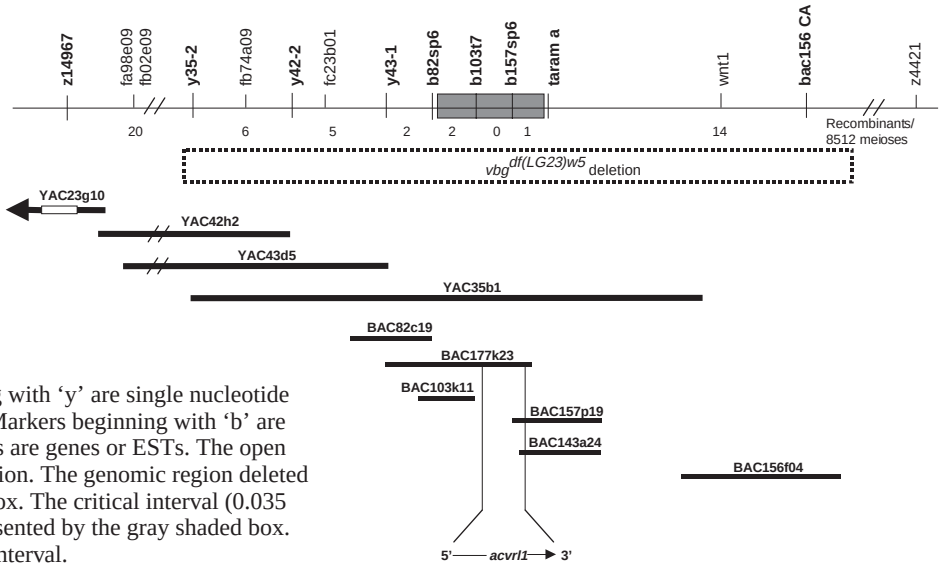

Fig. 3. Meiotic and physical map of the vbg interval on LG23. Markers that were meiotically mapped are shown in bold at the top of the figure, and the number of recombination breakpoints between these markers found after analysis of 8512 informative meioses is shown just below the line representing LG23. Markers that were only physically mapped or for which recombination was not assessed in all 8512 informative meioses are shown in plain type. Markers beginning with ‘z’ and bac156CA are SSLPs. Markers beginning with ‘y’ are single nucleotide polymorphisms (SNPs) found in YAC ends. Markers beginning with ‘b’ are SNPs found in BAC ends. Remaining markers are genes or ESTs. The open box in YAC23g10 represents an internal deletion. The genomic region deleted in *vbg*$^{df(LG23)w5}$ is represented by the dotted box. The critical interval (0.035 cM) defined by meiotic fine mapping is represented by the gray shaded box. The full *acvrl1* gene falls within this critical interval.

zehn1109 reveals a 499 amino acid protein with 55% identity to human and mouse Acvrl1 (Fig. 4). Homology to mammalian Acvrl1 is highest (75%) within the C-terminal kinase domain (from L196). Within this domain, the L45 loop (S254-S261), which confers Smad specificity to TGFβ type I receptors (Chen et al., 1998), contains only one conservative substitution. In contrast, the N-terminal ligand binding domain encoded by *zehn1109* shares only 17% identity with mammalian Acvrl1, most of which can be accounted for by ten cysteines that are common to all TGFβ type I receptors. Despite the lack of homology in the ligand binding domain, we strongly believe that this gene is the zebrafish ortholog of mammalian *Acvrl1* (see Discussion).

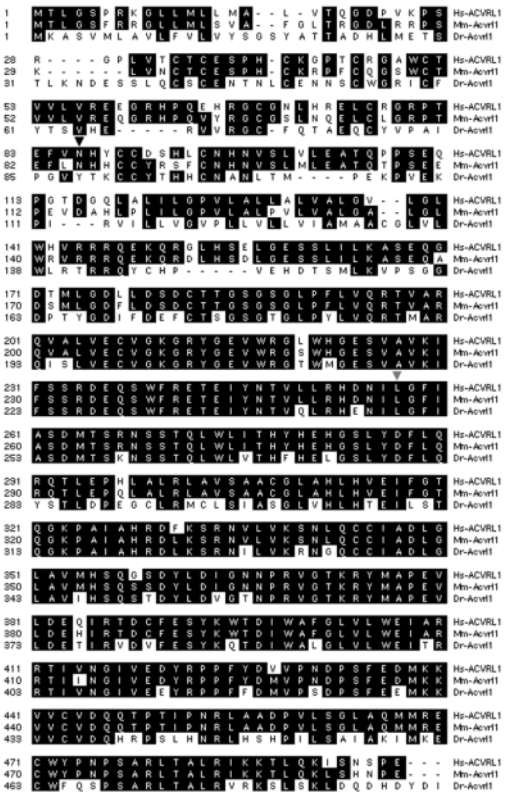

Fig. 4. Alignment of human (Hs-), mouse (Mm-), and zebrafish (Dr-) Acvrl1 proteins. Zebrafish *acvrl1* encodes a 499 amino acid protein with significant homology to mammalian Acvrl1 proteins in the C-terminal serine/threonine kinase domain. In contrast, although the ten cysteines common to all type I TGFβ receptors are conserved, the rest of the N-terminal ligand binding domain shows little homology. Black arrowhead, Y88Stop mutation in *vbg*^{ft09e}; gray arrowhead, L249F mutation in *vbg*^{y6}. GenBank accession numbers: *Danio rerio acvrl1* mRNA, complete cds; includes noncoding exon 1: AF435024. *Danio rerio acvrl1* mRNA, complete cds; no noncoding exon 1: AF435025.

Sequencing of *acvrl1* cDNA synthesized from *vbg*^{y6} mutant embryos uncovered a point mutation within the kinase domain creating a leucine-to-phenylalanine substitution (L249F; Fig. 4). This leucine, which lies five residues N-terminal to the L45 loop, is conserved in all TGFβ type I receptors, although it has not previously been ascribed a specific function. When assayed for this polymorphism, each *vbg*^{y6} mutant embryo recombinant at either of the closest flanking genomic markers was shown to possess the mutant genotype. Furthermore, sequencing of the *vbg*^{ft09e} allele revealed a point mutation converting a tyrosine to a stop codon (Y88Stop; Fig. 4). This mutation stops translation within the ligand binding domain and therefore would be expected to produce a nonfunctional protein.

To confirm that mutations in *acvrl1* are responsible for the *vbg* phenotype, we attempted to phenocopy this mutant using morpholino-modified antisense oligonucleotides (morpholinos) (Summerton, 1999). Morpholinos have been used in zebrafish to phenocopy a number of early mutations (Nasevicius and Ekker, 2000), and their stability allows translation inhibition relatively late in development. When injected into 1- to 4-cell wild-type embryos, a total of 22.5 ng of a control morpholino had no effect on blood flow or vascular architecture at 2.25 dpf (Fig. 5A). In contrast, 22.5 ng of a 2:1 mixture of *acvrl1* morpholinos directed against coding sequence (MO1) and noncoding exon1 (MO2) increased cranial blood flow relative to control in 86% (114/132) of embryos at 2.25 dpf. A 15 ng dose of morpholino mixture produced fewer embryos (11/50) with obvious phenotypes. Analysis of a random sample of affected embryos by confocal microangiography revealed a range of phenotypes, from essentially complete phenocopy of *vbg* mutants (Fig. 5B,C) to focal cranial vessel dilations (Fig. 5D). Affected vessels included the basal communicating artery, posterior connecting

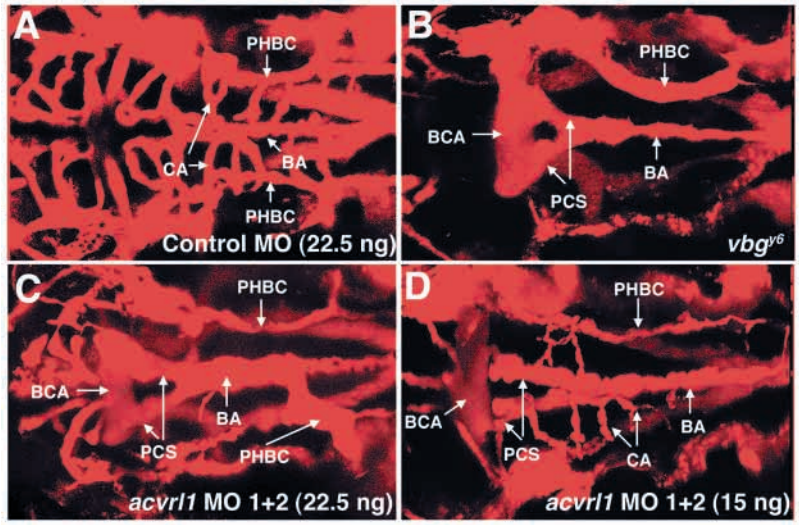

Fig. 5 Antisense morpholino-modified oligonucleotides directed against *acvrl1* phenocopy *vbg* mutants. Dorsal anterior angiograms of 2.25 dpf wild-type embryos injected at the 1- to 4-cell stage with 22.5 ng of a standard control morpholino (A) or 22.5 ng (C) or 15 ng (D) of a mixture of morpholinos directed against *acvrl1*. Note the strong resemblance of patent vessel architecture in C to that found in *vbg* mutants (B). The embryo shown in D is less severely affected but clearly shows dilated vessels and a decrease in the number of patent central arteries. BCA, basal communicating artery; PCS, posterior connecting segment; BA, basilar artery; PHBC, primordial hindbrain channel; CA, central artery. Dorsal views, anterior to the left.

segments, basilar artery, and primordial hindbrain channel, each of which can be dilated in *vbg* mutants.

Zebrafish *acvrl1* is expressed in endothelial cells

We used RT-PCR and whole-mount in situ hybridization to determine the temporal and spatial distribution of zebrafish *acvrl1* transcripts. By RT-PCR, *acvrl1* transcripts are first detectable at tailbud stage (10 hpf) and continue to be expressed as late as 4 dpf (data not shown). However, in situ hybridization is not sensitive enough to reliably detect *acvrl1* transcripts before 40-45 hpf. At this time, as in mammals, *acvrl1* is expressed in endothelial cells. Rostral *acvrl1* expression (Fig. 6A,B) is significantly weaker and more limited than that of the endothelial marker, *tie1* (Fig. 6E,F), and predominates in vessels that become enlarged in *vbg* mutants. *acvrl1* expression is strongest in the first aortic arch, the internal carotid artery and its caudal division, the basal communicating artery and the optic vein (Fig. 6A,B). The primordial hindbrain channels sometimes exhibit a weakly positive signal, whereas the basilar artery is consistently negative. The weak to undetectable staining of these latter vessels is also observed with *tie1* (Fig. 6E,F) and may reflect the inherent difficulty in staining deep cranial vessels using whole-mount in situ hybridization. *acvrl1* expression is moderate in the lateral dorsal aortae (Fig. 6B), weak in the trunk axial vessels, and undetectable in the trunk intersegmental vessels (Fig. 6C,D). Expression in these vessels is weaker but qualitatively identical to that of *tie1* (Fig. 6F,G,H).

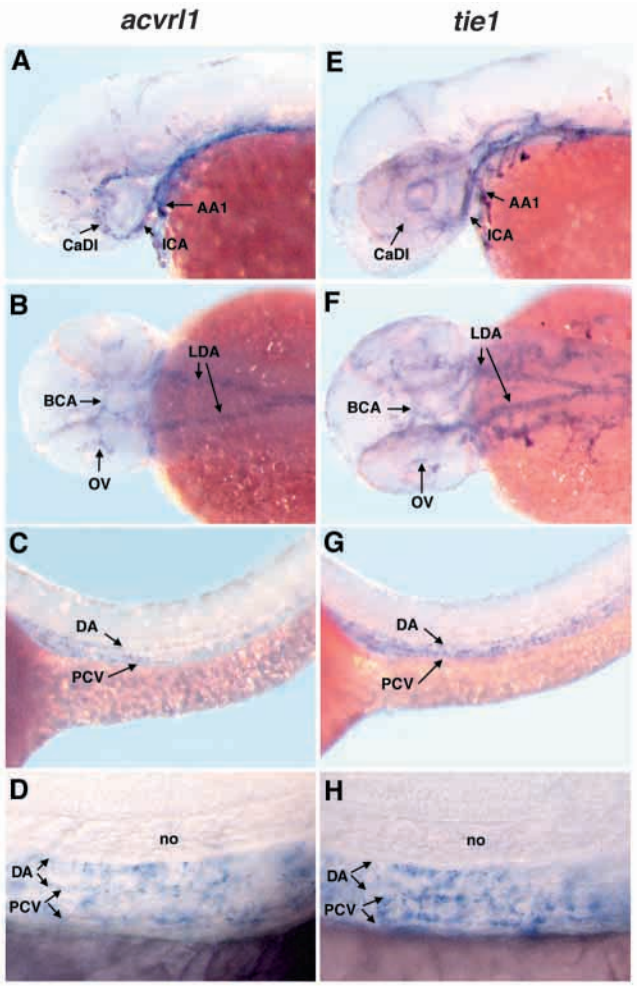

Fig. 6. Zebrafish *acvrl1* is expressed predominantly in the cranial blood vessels that become dilated in *vbg* mutants. Whole-mount in situ hybridization using *acvrl1* (A-D) or *tie1* (E-H) riboprobes on 40 hpf embryos. (A,B) Expression of *acvrl1* is strongest in cranial vessels, including the first arch artery (AA1), internal carotid artery (ICA), caudal division of the internal carotid artery (CaDI), basal communicating artery (BCA) and optic vein (OV). Expression in the lateral dorsal aortae (LDA) is moderate. (C,D) Very weak *acvrl1* expression is present in the dorsal aorta (DA) and posterior cardinal vein (PCV) (C, low magnification; D, high magnification). In general, *tie1* is more widely expressed in cranial endothelium (E,F) than *acvrl1*, although relative expression in the CaDI is weaker than *acvrl1* expression. In the LDA (F), DA and PCV (G, low magnification; H, high magnification), *tie1* expression is qualitatively similar to *acvrl1*. (A,C,D,E,G,H) Lateral view, anterior to the left. (B,F) Dorsal view, anterior to the left. no: notochord.

Zebrafish Acvrl1 signals through the Smad1/5/8 pathway

Mammalian Acvrl1 proteins signal through the Smad1/5/8, or BMP pathway, and not the Smad2/3, or TGFβ/activin/nodal pathway (Chen and Massague, 1999). To determine which Smad pathway is activated by zebrafish Acvrl1, we injected into 1- to 4-cell embryos activated *acvrl1* mRNA (*acvrl1**), which encodes a single amino change (Q193D) that renders Smad phosphorylation independent of ligand and type II receptor (Wieser et al., 1995). Injection of 5 pg *acvrl1** mRNA induces Smad1 phosphorylation at shield stage (6 hpf), as detected by whole-mount immunohistochemistry using a phospho-Smad1 antibody (Fig. 7A,B). Five pg of *acvrl1** also induces *gata2* mRNA (Fig. 7D,E), a ventral ectodermal marker that is upregulated by signaling through the Smad1/5/8 pathway (Maeno et al., 1996). In contrast, up to 100 pg mRNA of the vbg^{y6} allele of *acvrl1** (Q193D; L249F) is ineffective in inducing Smad1 phosphorylation and only minimally effective in inducing *gata2* mRNA expression (Fig. 7C,F) despite similar translation efficiencies of *acvrl1** and *acvrl1**(vbg^{y6}) mRNAs in vivo (data not shown).

BMPs, through the Smad1/5/8 pathway, play an important role in controlling dorsoventral patterning during early development. Thus, if zebrafish Acvrl1 does indeed signal through the Smad1/5/8 pathway, hyperactivation of the Acvrl1 pathway during gastrulation should ventralize embryos (Bauer et al., 2001; Kishimoto et al., 1997), whereas dominant negative inhibition should dorsalize embryos (Bauer et al., 2001; Hild et al., 1999; Mintzer et al., 2001). Of 116 surviving wild-type embryos injected with 1 pg *acvrl1** mRNA, 83% exhibited a ventralized phenotype (Kishimoto et al., 1997) at 24-30 hpf. Complete loss of anterior structures and notochord concomitant with expanded blood islands was the most frequently observed phenotype in these ventralized embryos (Fig. 7H; compare to control, Fig. 7G). Injection of 10 pg mRNA of the vbg^{y6} allele of *acvrl1** mildly ventralized only 9% of embryos (n=128), whereas 100 pg ventralized 41% of embryos (n=181), most of which exhibited incomplete loss of anterior structures and complete loss of notochord (Fig. 7I). Conversely, of 252 surviving embryos injected with 100 pg mRNA encoding a kinase-dead, dominant-negative form of Acvrl1 (Bassing et al., 1994)

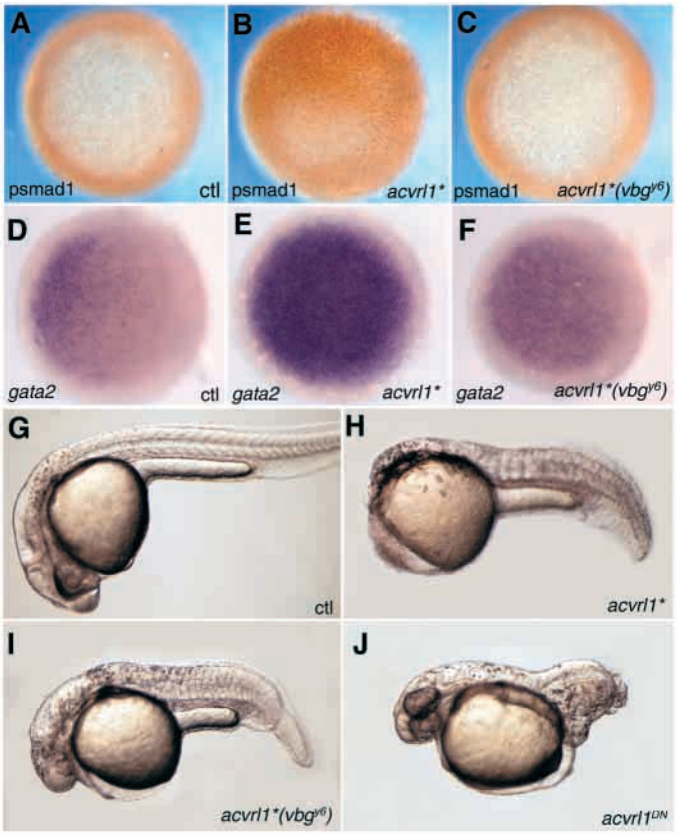

Fig. 7. Zebrafish Acvrl1 acts through the Smad1/5/8 pathway in vivo. Shield stage embryos injected at the 1- to 4-cell stage with 5 pg mRNA encoding an activated form of Acvrl1 (*acvrl1**) exhibit ectopic Smad1 phosphorylation (B) compared to uninjected controls (A). Expression of *gata2* is also upregulated in *acvrl1**-injected embryos (E) compared to uninjected controls (D). In contrast, 100 pg *acvrl1*(vbg^{y6})* mRNA was ineffective in inducing Smad1 phosphorylation (C), and only minimally effective in inducing *gata2* expression (F). When assayed at 24-30 hpf, embryos injected with 1 pg *acvrl1** mRNA (H) exhibited strong ventralization compared to uninjected controls (G), whereas those injected with 100 pg *acvrl1*(vbg^{y6})* mRNA were less severely ventralized (I). Embryos injected with 100 pg mRNA of a kinase-dead, dominant negative form of *acvrl1* (*acvrl1^{DN})* exhibit strong dorsalization (J), whereas those injected with 600 pg *acvrl1^{DN}(vbg^{y6})* were indistinguishable from wild type (data not shown). (A-F) Animal view; (G-J) lateral view, anterior to the left.

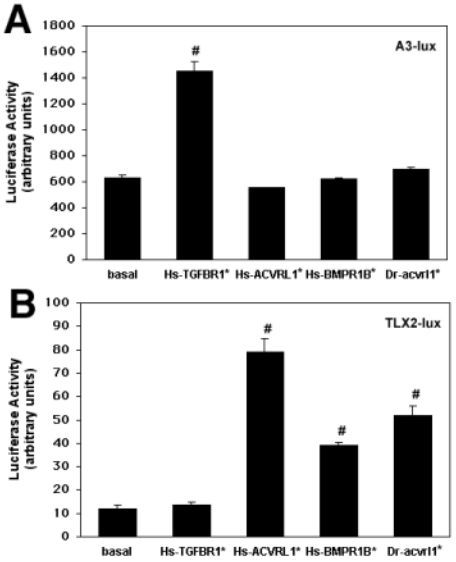

Fig. 8. Zebrafish Acvrl1 acts through the Smad1/5/8 pathway in cultured cells. P19 cells were transfected with a Smad2/3-responsive luciferase reporter, *pA3-lux* (A) or a Smad1/5/8-responsive luciferase reporter, *pTLX2-lux* (B), along with activated TGFβ type I receptors, Hs-*TGFBR1**, Hs-*ACVRL1**, Hs-*BMPR1B**, or Dr-*acvrl1**. Each bar represents mean±s.e.m. from 2 independent luciferase assays performed on each of 3 independent wells of transfected cells. #Significantly different from basal activity, $P<0.05$.

(*acvrl1^{DN};* K221R), 42% exhibited a dorsalized phenotype (Mullins et al., 1996) at 24 hpf. Severity of dorsalization ranged from embryos that lacked blood and exhibited a twisted trunk and no tail (Fig. 7J) to embryos in which the only abnormality noted was a small or absent tail fin (data not shown). In contrast, injection of 600 pg mRNA of the *vbg^{y6}* allele of *acvrl1^{DN}* (K221R; L249F) produced no phenotype (n=123; data not shown). These results provide further evidence that zebrafish Acvrl1, like mammalian Acvrl1, acts through the Smad1/5/8 pathway, and that the L249F mutation in the *vbg^{y6}* allele does indeed impair function of Acvrl1 protein.

The specificity of zebrafish Acvrl1 for the Smad1/5/8 pathway was confirmed in cultured cells. In P19 cells, luciferase transcription from the Smad2/3-responsive *A3* promoter is induced by human *TGFBR1**, but not human *ACVRL1**, human *BMPR1B** or zebrafish *acvrl1** (Fig. 8A). In contrast, luciferase transcription from the Smad1/5/8-responsive *TLX2* promoter is induced by human *ACVRL1**, human *BMPR1B**, and zebrafish *acvrl1** but not by human *TGFBR1** (Fig. 8B). These results confirm in vivo findings that zebrafish Acvrl1 signals through Smad1/5/8 and also demonstrate the inability of this receptor to signal through Smad2/3.

DISCUSSION

Using positional cloning and candidate gene testing, we have identified the molecular basis for the cranial vessel dilation observed in *vbg* mutants. We meiotically mapped the *vbg* locus to an interval of 0.035 cM on LG23 and established a physical contig across this region containing the *acvrl1* gene. The *vbg^{y6}* allele of *acvrl1* contains a missense mutation in the C-terminal serine/threonine kinase domain, whereas the *vbg^{ft09e}* allele contains a nonsense mutation in the N-terminal ligand binding domain. The former polymorphism exhibited no recombination in 4256 *vbg^{y6}* mutants (8512 informative meioses). Furthermore, injection of antisense, morpholino-modified oligonucleotides specific to *acvrl1* phenocopies the vascular defect seen in *vbg* mutants. Finally, at 40 hpf, when the *vbg* mutant phenotype is first detectable, *acvrl1* mRNA is expressed predominantly in vessels that are consistently dilated in *vbg* mutants: the first aortic arch, internal carotid artery/caudal division, and basal communicating artery. Taken together, these results support the conclusion that the

zebrafish *vbg* gene is *acvrl1*. It should be noted that injection of *acvrl1* mRNA at the 1- to 4-cell stage was unable to rescue the *vbg* mutant phenotype owing to instability of injected mRNA and/or translated protein; Acvrl1-myc fusion proteins were undetectable by 24 hpf (data not shown).

Although the zebrafish gene residing at the *vbg* locus is highly homologous to mammalian Acvrl1 in the kinase domain and in particular in the L45 loop, it shows little homology to any TGFβ type I receptor in the ligand binding domain: only ten cysteines that are common to all TGFβ type I receptors are conserved. However, we feel that it is appropriate to call the *vbg* gene *acvrl1* for a number of reasons. First, human *ACVRL1* is located on chromosome 12q13 (Johnson et al., 1996), which shows conserved synteny with the region surrounding the *vbg* locus on zebrafish LG23 (Postlethwait et al., 1998). Second, like mammalian *Acvrl1* (Johnson et al., 1996; Oh et al., 2000; Roelen et al., 1997; Urness et al., 2000), the *vbg* gene is expressed predominantly if not exclusively in endothelial cells, and *vbg* disruption results in vascular defects. Third, both mammalian Acvrl1 (Chen and Massague, 1999) and the *vbg* gene product signal through the Smad1/5/8 pathway, and not the Smad2/3 pathway. And fourth, a lack of homology within the ligand binding domain has also been observed for the zebrafish TGFβ type I receptors, Alk8 (Mintzer et al., 2001; Payne et al., 2001; Yelick et al., 1998) and Taram-A (Renucci et al., 1996). Based on conserved synteny, L45 loop sequence, and Smad specificity, Alk8 and Taram-A seem to be orthologs of mammalian Acvr1 and Acvr1b, respectively.

While the premature stop codon in the ligand binding domain generated by the vbg^{ft09e} mutation most likely produces a nonfunctional Acvrl1 protein, the consequence of the L249F substitution produced by the vbg^{y6} mutation is not self-evident. However, the resulting phenotype, which is indistinguishable from vbg^{ft09e}, suggests that L249 is critical for Acvrl1 protein function. Although in vivo assays using an activated form of the vbg^{y6} allele of *acvrl1* suggest that it retains some activity, the artificial activation of this protein, allowing it to function independently of ligand and type II receptor, makes its true in vivo efficacy difficult to gauge. Activity of the non-activated vbg^{y6} allele could not be assayed because injection of either wild-type or vbg^{y6} mutant *acvrl1* mRNA produced no phenotype in wild-type embryos (data not shown). The lack of effect of injection of mRNA encoding a TGFβ type I receptor has been previously reported (Bauer et al., 2001) and suggests that pathway activity is limited by ligand or type II receptor.

The three *vbg* alleles analyzed in this study exhibit similar vascular phenotypes characterized by dilated cranial vessels that carry the bulk of blood flow. The cause of this vessel dilation is an increase in the number of endothelial cells within affected vessels, suggesting that Acvrl1 signaling may inhibit endothelial cell proliferation and promote vessel stabilization. While there is some in vivo evidence that TGFβ family signaling in general (and Acvrl1 signaling specifically) plays a role in vessel stabilization via vascular smooth muscle cell recruitment and differentiation (Larsson et al., 2001; Li et al., 1999; Oh et al., 2000; Oshima et al., 1996; Urness et al., 2000; Yang et al., 1999), the dilated first aortic arch, internal carotid artery, and caudal division of the internal carotid artery in *vbg* mutants normally express the vascular smooth muscle cell marker, *sm22α*, at 2 dpf (data not shown). These data suggest that in zebrafish, the *acvrl1* mutation-induced increases in endothelial cell number and vessel caliber are not correlated with vascular smooth muscle deficits. A similar phenomenon has recently been reported as a result of misexpression of Smad7, an inhibitory Smad that blocks signaling mediated by all receptor-specific Smads (Vargesson and Laufer, 2001).

The cross-species conservation of *acvrl1* expression pattern and function suggests that the mechanism underlying vessel dilation in zebrafish *vbg* mutants is most likely similar to that underlying vessel dilation – the first step in telangiectasia and AVM formation (Braverman et al., 1990) – in HHT2 patients. Thus, although the enlarged cranial vessels in *vbg* mutants are not precursors of AVMs per se (the malformations seen in *vbg* mutants appear to be normal, primitive connections that are aberrantly retained), an understanding of their etiology should lead to insight into the mechanism of HHT2-associated vascular lesions. Although it has been proposed (Urness et al., 2000) that the proximal event leading to AVMs in an *Acvrl1* null mouse is loss of arterial identity, as assayed by loss of arterial *ephrinB2* expression, vessel dilation in these mice (E8.0) precedes the onset of normal arterial *ephrinB2* expression (E8.25) (Wang et al., 1998b) and AVM formation (E8.5), suggesting that in mice, too, the earliest manifestation of loss of *Acvrl1* expression is vessel dilation. It should be noted that *vbg* mutants express *ephrinB2* normally in the dorsal aorta (data not shown); expression in cranial arteries, which are dilated in *vbg* mutants, could not be assessed by whole-mount in situ hybridization because of intense staining of other cranial structures.

While it is clear that the genetic lesion responsible for HHT2 is a mutation in *ACVRL1*, the age of onset, location, and severity of clinical manifestations of this autosomal dominant disorder vary greatly among heterozygous carriers. While it remains possible that loss of heterozygosity plays a role in determining lesion location, this phenomenon could not be demonstrated in lesions associated with the related disorder, HHT1 (Bourdeau et al., 2000a). Thus, in both diseases, additional genetic and/or environmental factors most likely come into play. While preliminary analysis of $vbg^{y6/+}$ fish has revealed no obvious superficial telangiectases or hemorrhages, it remains possible that such defects might manifest in certain genetic backgrounds [as in *Eng* haploinsufficiency in mice (Bourdeau et al., 1999; Bourdeau et al., 2000b)], or that mutagenesis screening might help to define genetic modifiers that render *acvrl1* haploinsufficiency symptomatic in zebrafish as well as in humans. Mutagenesis screens might also produce complementing mutations that may lead to discovery of upstream or downstream components of the Acvrl1 signaling pathway. Furthermore, *vbg* mutants should prove useful in describing the consequences of *acvrl1* deficiency in terms of endothelial cell behavior, as vessel formation can be documented in real time in transgenic lines such as $TG(fli1{:}nEGFP)^{y7}$. Thus, like a number of other zebrafish models of human diseases (Brownlie et al., 1998; Childs et al., 2000; Wang et al., 1998a), this zebrafish model of HHT2 provides a powerful tool that should complement established mouse models in the study of disease etiology and the development of treatment strategies.

We thank N. Hukriede for assistance with radiation hybrid mapping, supplying the SMART RACE library, and helpful discussions; S. Isogai for microangiography training; C. Abnet for statistical advice; R. Subramanian for critical review of the manuscript; A. Chin and P. Bennett for fish care; and M. Kawabata, K. Peters, M. Tsang, M. Whitman, J. Wrana, and L. Zon for plasmids. This work was funded by NIH Z01-HD-01011 (to B. M. W.) and HL65681 (to R. J. L.).

REFERENCES

Barbara, N. P., Wrana, J. L. and Letarte, M. (1999). Endoglin is an accessory protein that interacts with the signaling receptor complex of multiple members of the transforming growth factor-β superfamily. *J. Biol. Chem.* **274**, 584-594.

Bassing, C. H., Yingling, J. M., Howe, D. J., Wang, T., He, W. W., Gustafson, M. L., Shah, P., Donahoe, P. K. and Wang, X. F. (1994). A transforming growth factor β type I receptor that signals to activate gene expression. *Science* **263**, 87-89.

Bauer, H., Lele, Z., Rauch, G. J., Geisler, R. and Hammerschmidt, M. (2001). The type I serine/threonine kinase receptor Alk8/Lost-a-fin is required for Bmp2b/7 signal transduction during dorsoventral patterning of the zebrafish embryo. *Development* **128**, 849-858.

Berg, J. N., Gallione, C. J., Stenzel, T. T., Johnson, D. W., Allen, W. P., Schwartz, C. E., Jackson, C. E., Porteous, M. E. and Marchuk, D. A. (1997). The activin receptor-like kinase 1 gene: genomic structure and mutations in hereditary hemorrhagic telangiectasia type 2. *Am. J. Hum. Genet.* **61**, 60-67.

Bourdeau, A., Cymerman, U., Paquet, M. E., Meschino, W., McKinnon, W. C., Guttmacher, A. E., Becker, L. and Letarte, M. (2000a). Endoglin expression is reduced in normal vessels but still detectable in arteriovenous malformations of patients with hereditary hemorrhagic telangiectasia type 1. *Am. J. Pathol.* **156**, 911-923.

Bourdeau, A., Dumont, D. J. and Letarte, M. (1999). A murine model of hereditary hemorrhagic telangiectasia. *J. Clin. Invest.* **104**, 1343-1351.

Bourdeau, A., Faughnan, M. E. and Letarte, M. (2000b). Endoglin-deficient mice, a unique model to study hereditary hemorrhagic telangiectasia. *Trends Cardiovasc. Med.* **10**, 279-285.

Braverman, I. M., Keh, A. and Jacobson, B. S. (1990). Ultrastructure and three-dimensional organization of the telangiectases of hereditary hemorrhagic telangiectasia. *J. Invest. Dermatol*. **95**, 422-427.

Brownlie, A., Donovan, A., Pratt, S. J., Paw, B. H., Oates, A. C., Brugnara, C., Witkowska, H. E., Sassa, S. and Zon, L. I. (1998). Positional cloning of the zebrafish *sauternes* gene: a model for congenital sideroblastic anaemia. *Nature Genet.* **20**, 244-250.

Chen, J. N., van Bebber, F., Goldstein, A. M., Serluca, F. C., Jackson, D., Childs, S., Serbedzija, G. N., Warren, K. S., Mably, J. D., Lindahl, P. et al. (2001). Genetic steps to organ laterality in zebrafish. *Comp. Funct. Genet.* **2**, 60-68.

Chen, Y. G., Hata, A., Lo, R. S., Wotton, D., Shi, Y., Pavletich, N. and Massague, J. (1998). Determinants of specificity in TGF-β signal transduction. *Genes Dev.* **12**, 2144-2152.

Chen, Y. G. and Massague, J. (1999). Smad1 recognition and activation by the ALK1 group of transforming growth factor-β family receptors. *J. Biol. Chem.* **274**, 3672-3677.

Childs, S., Weinstein, B. M., Mohideen, M. A., Donohue, S., Bonkovsky, H. and Fishman, M. C. (2000). Zebrafish *dracula* encodes ferrochelatase and its mutation provides a model for erythropoietic protoporphyria. *Curr. Biol.* **10**, 1001-1004.

Detrich, H. W., 3rd, Kieran, M. W., Chan, F. Y., Barone, L. M., Yee, K., Rundstadler, J. A., Pratt, S., Ransom, D. and Zon, L. I. (1995). Intraembryonic hematopoietic cell migration during vertebrate development. *Proc. Natl. Acad. Sci. USA* **92**, 10713-10717.

Dickson, M. C., Martin, J. S., Cousins, F. M., Kulkarni, A. B., Karlsson, S. and Akhurst, R. J. (1995). Defective haematopoiesis and vasculogenesis in transforming growth factor-β1 knock out mice. *Development* **121**, 1845-1854.

Driever, W., Solnica-Krezel, L., Schier, A. F., Neuhauss, S. C., Malicki, J., Stemple, D. L., Stainier, D. Y., Zwartkruis, F., Abdelilah, S., Rangini, Z. et al. (1996). A genetic screen for mutations affecting embryogenesis in zebrafish. *Development* **123**, 37-46.

Guttmacher, A. E., Marchuk, D. A. and White, R. I., Jr (1995). Hereditary hemorrhagic telangiectasia. *N. Engl. J. Med.* **333**, 918-924.

Hauptmann, G. and Gerster, T. (1994). Two-color whole-mount in situ hybridization to vertebrate and *Drosophila* embryos. *Trends Genet.* **10**, 266.

Hild, M., Dick, A., Rauch, G. J., Meier, A., Bouwmeester, T., Haffter, P. and Hammerschmidt, M. (1999). The *smad5* mutation *somitabun* blocks Bmp2b signaling during early dorsoventral patterning of the zebrafish embryo. *Development* **126**, 2149-2159.

Hukriede, N. A., Joly, L., Tsang, M., Miles, J., Tellis, P., Epstein, J. A., Barbazuk, W. B., Li, F. N., Paw, B., Postlethwait, J. H. et al. (1999). Radiation hybrid mapping of the zebrafish genome. *Proc. Natl. Acad. Sci. USA* **96**, 9745-9750.

Isogai, S., Horiguchi, M. and Weinstein, B. M. (2001). The vascular anatomy of the developing zebrafish: an atlas of embryonic and early larval development. *Dev. Biol.* **230**, 278-301.

Johnson, D. W., Berg, J. N., Baldwin, M. A., Gallione, C. J., Marondel, I., Yoon, S. J., Stenzel, T. T., Speer, M., Pericak-Vance, M. A., Diamond, A. et al. (1996). Mutations in the activin receptor-like kinase 1 gene in hereditary haemorrhagic telangiectasia type 2. *Nature Genet.* **13**, 189-195.

Kimmel, C. B., Ballard, W. W., Kimmel, S. R., Ullmann, B. and Schilling, T. F. (1995). Stages of embryonic development in the zebrafish. *Dev. Dynam.* **203**, 253-310.

Kishimoto, Y., Lee, K. H., Zon, L., Hammerschmidt, M. and Schulte-Merker, S. (1997). The molecular nature of zebrafish *swirl*: BMP2 function is essential during early dorsoventral patterning. *Development* **124**, 4457-4466.

Knapik, E. W., Goodman, A., Ekker, M., Chevrette, M., Delgado, J., Neuhauss, S., Shimoda, N., Driever, W., Fishman, M. C. and Jacob, H. J. (1998). A microsatellite genetic linkage map for zebrafish (*Danio rerio*). *Nature Genet.* **18**, 338-343.

Larsson, J., Goumans, M. J., Sjostrand, L. J., van Rooijen, M. A., Ward, D., Leveen, P., Xu, X., ten Dijke, P., Mummery, C. L. and Karlsson, S. (2001). Abnormal angiogenesis but intact hematopoietic potential in TGF-β type I receptor-deficient mice. *EMBO J.* **20**, 1663-1673.

Lawson, N. D., Scheer, N., Pham, V. N., Kim, C. H., Chitnis, A. B., Campos-Ortega, J. A. and Weinstein, B. M. (2001). Notch signaling is required for arterial-venous differentiation during embryonic vascular development. *Development* **128**, 3675-3683.

Lekven, A. C., Helde, K. A., Thorpe, C. J., Rooke, R. and Moon, R. T. (2000). Reverse genetics in zebrafish. *Physiol. Genomics* **2**, 37-48.

Li, D. Y., Sorensen, L. K., Brooke, B. S., Urness, L. D., Davis, E. C., Taylor, D. G., Boak, B. B. and Wendel, D. P. (1999). Defective angiogenesis in mice lacking endoglin. *Science* **284**, 1534-1537.

Lux, A., Attisano, L. and Marchuk, D. A. (1999). Assignment of transforming growth factor β1 and β3 and a third new ligand to the type I receptor ALK-1. *J. Biol. Chem.* **274**, 9984-9992.

Lyons, M. S., Bell, B., Stainier, D. and Peters, K. G. (1998). Isolation of the zebrafish homologues for the *tie-1* and *tie-2* endothelium-specific receptor tyrosine kinases. *Dev. Dyn.* **212**, 133-140.

Macias-Silva, M., Hoodless, P. A., Tang, S. J., Buchwald, M. and Wrana, J. L. (1998). Specific activation of Smad1 signaling pathways by the BMP7 type I receptor, ALK2. *J. Biol. Chem.* **273**, 25628-25636.

Maeno, M., Mead, P. E., Kelley, C., Xu, R. H., Kung, H. F., Suzuki, A., Ueno, N. and Zon, L. I. (1996). The role of BMP-4 and GATA-2 in the induction and differentiation of hematopoietic mesoderm in *Xenopus laevis*. *Blood* **88**, 1965-1972.

Massague, J., Blain, S. W. and Lo, R. S. (2000). TGFβ signaling in growth control, cancer, and heritable disorders. *Cell* **103**, 295-309.

McAllister, K. A., Grogg, K. M., Johnson, D. W., Gallione, C. J., Baldwin, M. A., Jackson, C. E., Helmbold, E. A., Markel, D. S., McKinnon, W. C., Murrell, J. et al. (1994). Endoglin, a TGF-β binding protein of endothelial cells, is the gene for hereditary haemorrhagic telangiectasia type 1. *Nature Genet.* **8**, 345-351.

McDonald, J. E., Miller, F. J., Hallam, S. E., Nelson, L., Marchuk, D. A. and Ward, K. J. (2000). Clinical manifestations in a large hereditary hemorrhagic telangiectasia (HHT) type 2 kindred. *Am. J. Med. Genet.* **93**, 320-327.

Mintzer, K. A., Lee, M. A., Runke, G., Trout, J., Whitman, M. and Mullins, M. C. (2001). *lost-a-fin* encodes a type I BMP receptor, Alk8, acting maternally and zygotically in dorsoventral pattern formation. *Development* **128**, 859-869.

Mullins, M. C., Hammerschmidt, M., Kane, D. A., Odenthal, J., Brand, M., van Eeden, F. J., Furutani-Seiki, M., Granato, M., Haffter, P.,

Heisenberg, C. P. et al. (1996). Genes establishing dorsoventral pattern formation in the zebrafish embryo: the ventral specifying genes. *Development* **123**, 81-93.

Nasevicius, A. and Ekker, S. C. (2000). Effective targeted gene 'knockdown' in zebrafish. *Nature Genet.* **26**, 216-220.

Neff, M. M., Neff, J. D., Chory, J. and Pepper, A. E. (1998). dCAPS, a simple technique for the genetic analysis of single nucleotide polymorphisms: experimental applications in *Arabidopsis thaliana* genetics. *Plant J.* **14**, 387-392.

Oh, S. P., Seki, T., Goss, K. A., Imamura, T., Yi, Y., Donahoe, P. K., Li, L., Miyazono, K., ten Dijke, P., Kim, S. et al. (2000). Activin receptor-like kinase 1 modulates transforming growth factor-β1 signaling in the regulation of angiogenesis. *Proc. Natl. Acad. Sci. USA* **97**, 2626-2631.

Oshima, M., Oshima, H. and Taketo, M. M. (1996). TGF-β receptor type II deficiency results in defects of yolk sac hematopoiesis and vasculogenesis. *Dev. Biol.* **179**, 297-302.

Payne, T. L., Postlethwait, J. H. and Yelick, P. C. (2001). Functional characterization and genetic mapping of *alk8*. *Mech. Dev.* **100**, 275-289.

Postlethwait, J. H., Yan, Y. L., Gates, M. A., Horne, S., Amores, A., Brownlie, A., Donovan, A., Egan, E. S., Force, A., Gong, Z. et al. (1998). Vertebrate genome evolution and the zebrafish gene map. *Nature Genet.* **18**, 345-349.

Renucci, A., Lemarchandel, V. and Rosa, F. (1996). An activated form of type I serine/threonine kinase receptor TARAM-A reveals a specific signalling pathway involved in fish head organiser formation. *Development* **122**, 3735-3743.

Roelen, B. A., van Rooijen, M. A. and Mummery, C. L. (1997). Expression of ALK-1, a type 1 serine/threonine kinase receptor, coincides with sites of vasculogenesis and angiogenesis in early mouse development. *Dev. Dyn.* **209**, 418-430.

Roman, B. L. and Weinstein, B. M. (2000). Building the vertebrate vasculature: research is going swimmingly. *BioEssays* **22**, 882-893.

Rupp, R. A., Snider, L. and Weintraub, H. (1994). *Xenopus* embryos regulate the nuclear localization of XMyoD. *Genes Dev.* **8**, 1311-1323.

Summerton, J. (1999). Morpholino antisense oligomers: the case for an RNase H-independent structural type. *Biochim. Biophys. Acta* **1489**, 141-158.

Urness, L. D., Sorensen, L. K. and Li, D. Y. (2000). Arteriovenous malformations in mice lacking activin receptor-like kinase-1. *Nature Genet.* **26**, 328-331.

Vargesson, N. and Laufer, E. (2001). Smad7 misexpression during embryonic angiogenesis causes vascular dilation and malformations independently of vascular smooth muscle cell function. *Dev. Biol.* **240**, 499-516.

Wang, H., Long, Q. M., Marty, S. D., Sassa, S. and Lin, S. (1998a). A zebrafish model for hepatoerythropoietic porphyria. *Nature Genet.* **20**, 239-243.

Wang, H. U., Chen, Z. F. and Anderson, D. J. (1998b). Molecular distinction and angiogenic interaction between embryonic arteries and veins revealed by ephrin-B2 and its receptor Eph-B4. *Cell* **93**, 741-753.

Weinstein, B. M., Stemple, D. L., Driever, W. D. and Fishman, M. C. (1995). *gridlock*, a localized heritable vascular patterning defect in the zebrafish. *Nature Med.* **11**, 1143-1147.

Westerfield, M. (1995). *The Zebrafish Book*. Eugene: University of Oregon Press.

Wieser, R., Wrana, J. L. and Massague, J. (1995). GS domain mutations that constitutively activate TβR-I, the downstream signaling component in the TGF-β receptor complex. *EMBO J.* **14**, 2199-2208.

Yang, X., Castilla, L. H., Xu, X., Li, C., Gotay, J., Weinstein, M., Liu, P. P. and Deng, C. X. (1999). Angiogenesis defects and mesenchymal apoptosis in mice lacking SMAD5. *Development* **126**, 1571-1580.

Yelick, P. C., Abduljabbar, T. S. and Stashenko, P. (1998). zALK-8, a novel type I serine/threonine kinase receptor, is expressed throughout early zebrafish development. *Dev. Dyn.* **211**, 352-361.

Yue, J., Hartsough, M. T., Frey, R. S., Frielle, T. and Mulder, K. M. (1999). Cloning and expression of a rat Smad1: regulation by TGFβ and modulation by the Ras/MEK pathway. *J. Cell Physiol.* **178**, 387-396.